Drug Design, Development and Therapy Dovepress

Open Access Full Text Article ORIGINAL RESEARCH

Magnetic-Powered Spora Lygodii Microrobots Loaded with Doxorubicin for Active and Targeted Therapy of Bladder Cancer

Qingxin Yang[1–3], Wen Yuan[2], Tinghui Zhao[4], Yanixao Jiao[5], Menghuan Tang[5], Zhaoqing Cong[5,6], Song Wu[6]

[1]Department of Pharmacy, Mianyang Orthopaedic Hospital, Mianyang, 621000, People's Republic of China; [2]Mianyang Key Laboratory of Development and Utilization of Chinese Medicine Resources, Mianyang, 621000, People's Republic of China; [3]The Third Affiliated Hospital of Shenzhen University, Shenzhen Luohu People's Hospital, Shenzhen, 518000, People's Republic of China; [4]Department of Burns and Plastic Surgery, Mianyang Central Hospital, Mianyang, 621000, People's Republic of China; [5]Department of Biochemistry and Molecular Medicine, University of California, Davis, CA, 95817, USA; [6]South China Hospital, Medical School, Shenzhen University, Shenzhen, 518116, People's Republic of China

Correspondence: Song Wu; Zhaoqing Cong, Email wusong@szu.edu.cn; zcong@ucdavis.edu

Background and Purpose: Bladder cancer has high recurrence rates despite standard treatments, necessitating innovative therapeutic approaches. This study introduces magnetically powered microrobots utilizing Traditional Chinese Medicine (TCM) Spora Lygodii (SL) encapsulated with Doxorubicin (DOX) and Fe_3O_4 nanoparticles (Fe/DOX@SL) for targeted therapy.

Methods: Fe_3O_4 nanoparticles were synthesized via co-precipitation and combined with SL spores and DOX through dip-coating to form Fe/DOX@SL microrobots. Their propulsion was controlled by a rotating magnetic field (RMF) for precise delivery. The microrobots' mobility and adherence were assessed in various biological media. Therapeutic efficacy was evaluated using an orthotopic bladder cancer model in mice treated intravesically with Fe/DOX@SL under RMF guidance, compared to controls.

Results: Fe/DOX@SL microrobots demonstrated efficient movement and stable navigation in biological environments. In vivo experiments showed superior retention in the bladder, prolonged adherence to the mucosa, and significantly enhanced tumor suppression in the RMF-guided group. Bioluminescence imaging confirmed reduced tumor growth, and histological analysis revealed substantial tumor regression compared to other treatments.

Discussion and Conclusion: This study highlights the potential of integrating TCM with advanced microrobotics. The biocompatible Fe/DOX@SL microrobots leverage SL's therapeutic properties and fuel-free magnetic control to overcome challenges in bladder cancer treatment, such as poor drug retention and off-target toxicity. This novel platform represents a promising advancement in targeted cancer therapy. The innovative fusion of TCM and microrobotics introduces a potent, targeted therapeutic strategy for bladder cancer, paving the way for broader biomedical applications.

Keywords: Traditional Chinese Medicine (TCM), Spora Lygodii, microrobots, bladder cancer

Introduction

Microrobots are emerging as a revolutionary tool in fields like biomedical engineering[1,2] and environmental remediation,[3] offering versatile applications ranging from cargo manipulation and environmental clean-up to targeted medical therapies. In the design of these micromachines, the biocompatibility and biodegradability of their constituent materials are paramount.[4] Ideally, these materials should be able to degrade harmlessly in biological environments, thereby eliminating the need for a post-use removal process. Biodegradable materials are especially favored in design, as they naturally break down into non-toxic substances, posing minimal risk to the human body when used in moderate quantities.[5,6] However, in the relatively mild conditions of biological environments, only a limited range of materials exhibit this desired biodegradability.[7] Recent developments in biodegradable micromachines have seen the use of both inorganic materials like metal-organic framework (MOF),[1,8] reactive metals,[4,5] and organic materials.[9–11] These materials

Received: 29 September 2024
Accepted: 29 November 2024
Published: 7 December 2024

serve as the building blocks or functional layers for applications in living organisms, underscoring the potential of microrobots in both medical and environmental applications. This focus on biodegradability and biocompatibility[12] is integral to the sustainable and safe implementation of microrobot technology.

Traditional Chinese Medicine (TCM) represents a significant cultural heritage, reflecting the Chinese people's extensive experience in combating diseases.[13] Practitioners of TCM use a variety of Chinese Medicinal Materials (CMMs), obtained from plant and animal sources, for the prevention, diagnosis, and treatment of various diseases.[14–16] Among these, plant spores are particularly noted for their roles in boosting immunity, treating cardiovascular diseases, and in tumor therapy.[17] Plant spores are inherently stable and possess a porous structure, making them exceptionally effective for drug loading and detoxification purposes.[18,19] This is due to their ability to maintain a sustainable and porous form, which facilitates efficient drug absorption and release. Although we have previously reported on the use of Pollen Typha as microrobots,[20] research on spores, in general, remains relatively limited.

This gap in research highlights the potential for further exploration into the use of spores within TCM, especially considering their natural structural advantages for medical applications. The inherent characteristics of spores – stability, porosity, and sustainability – make them promising candidates for innovative medical treatments, including the development of new forms of microrobots for targeted therapies. This area offers a fertile ground for advancing TCM practices and integrating them with modern technological approaches.

Bladder cancer is among the top ten most common cancers globally, with approximately 75% of cases initially diagnosed as non-muscle invasive.[21,22] The usual treatment is transurethral resection, though this approach has a high recurrence rate, with up to 70% of patients relapsing within five years. To reduce recurrence, intravesical chemotherapy is often used, but it faces challenges such as poor targeting of cancer cells, toxicity to healthy tissues, and short drug retention time in the bladder. These limitations result in side effects, reduced treatment effectiveness, and the need for multiple procedures, increasing patient burden and healthcare costs.[23,24] Recent advancements have introduced urease-powered micromotors for in vitro therapy of 3D bladder cancer spheroids and in vivo bladder imaging.[25] However, despite the propulsion provided by their enzymatic engines, these micromotors still experience limited mobility and control. The demand for more effective treatments remains, prompting ongoing research into microrobots with fuel-free propulsion, precise navigation, and the ability to selectively target and destroy bladder tumors.

This study introduces a groundbreaking therapeutic microrobotic platform that ingeniously integrates Traditional Chinese Medicine (TCM) with advanced microrobotics for effective bladder cancer treatment (Figure 1). Doxorubicin (DOX) is a widely used chemotherapy drug for bladder cancer treatment; however, its severe side effects significantly limit its clinical application. To address these challenges, several studies have explored loading DOX onto metal nanoparticles to enhance its antitumor efficacy while minimizing systemic toxicity.[26,27] Among these, Fe_3O_4 nanoparticles (NPs) have demonstrated excellent biocompatibility,[28] making them a promising candidate for drug delivery systems. Spora Lygodii (SL), the dried spore of Lygodium japonicum (Thunb.) Sw., is not only renowned in TCM for its therapeutic properties—such as clearing heat, promoting urination, relieving painful urinary dysfunction, expelling stones, eliminating damp-heat, reducing edema, and alleviating jaundice—but also possesses a naturally porous structure that is particularly advantageous for biomedical applications.[29,30] This porous architecture enables efficient drug loading and controlled release, making it an ideal carrier for encapsulating DOX and Fe_3O_4 NPs)through a straightforward dip-coating method. Furthermore, its inherent biocompatibility and therapeutic potential complement its role as a dual-function material, serving both as a drug delivery vehicle and as a contributor to the overall therapeutic effect, aligning with the study's goal of integrating TCM with cutting-edge microrobotics for targeted cancer therapy. This unique combination of structural and pharmacological attributes makes SL a compelling choice for this application. Dox is a classical chemodrug for bladder cancer therapy, however, the severe side effect higly limit its application. Several attempts has reported to load the DOX with metal nanoparticles to get better antitumor effect. The fe3O4 NPs has shown superior biocompatibility. This process results in the creation of innovative Fe/DOX@SL microrobots. These microrobots are engineered to exhibit accurate, stable, and controllable movement across different biological environments, directed by an external rotating magnetic field (RMF). A key feature of the Fe/DOX@SL microrobots is their ability to navigate and sustain their presence within a mouse's bladder, controlled remotely by magnetic manipulation. This technique significantly enhances the microrobots' adherence to the bladder mucosa and extends their retention, thereby

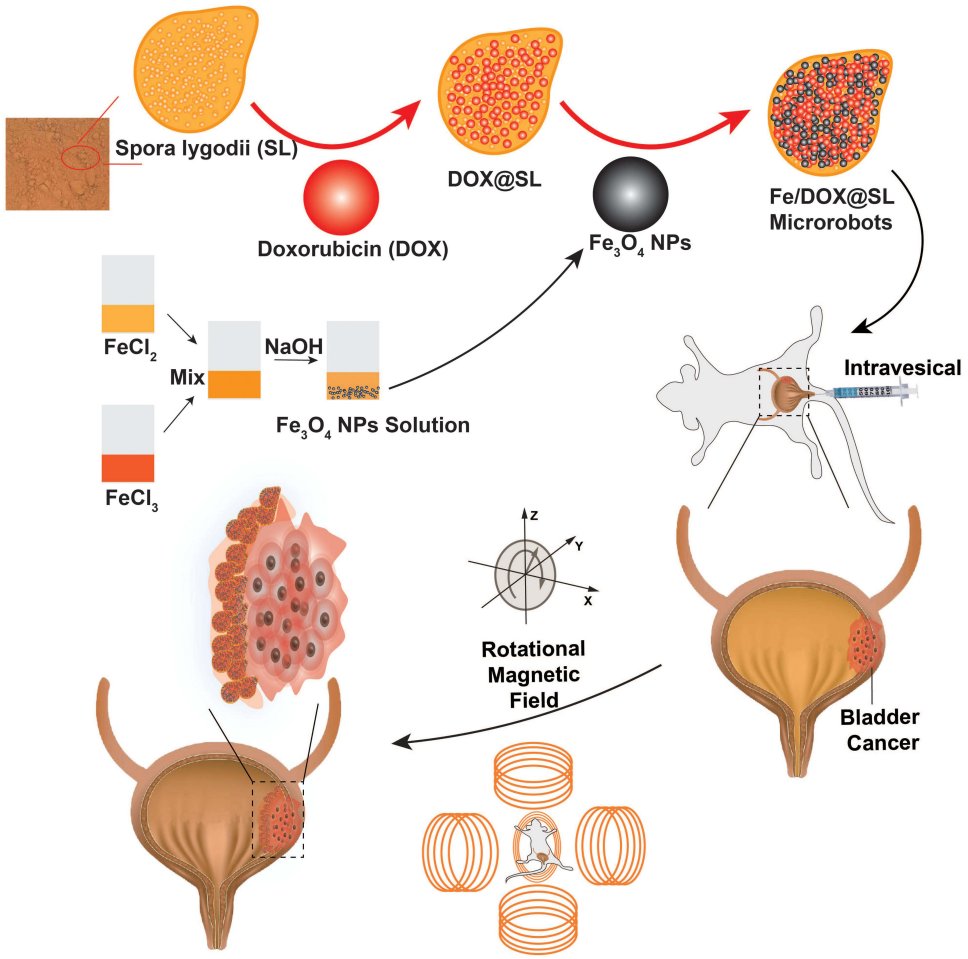

Figure 1 Illustration of the magnetic-powered spora lygodii (SL) microrobots loaded with doxorubicin (DOX) for active and targeted therapy of bladder cancer.

boosting their therapeutic efficacy. In experiments involving mice with T24 bladder tumors, these magnetically steered SL microrobots exhibited a markedly improved anti-tumor effect compared to other passive treatments. This research leverages the innate properties of SL spores to develop biocompatible microrobots with intrinsic healing capabilities and a fuel-free, controllable propulsion mechanism. It opens a new and promising pathway for the effective treatment of bladder cancer. The innovative fusion of TCM elements with cutting-edge microrobot technology in this study has the potential to initiate a new paradigm in cancer treatment methodologies.

Materials and Methods

Preparation and Characterization of Fe_3O_4 NPs

Fe_3O_4 NPs were synthesized through a co-precipitation method in an ultrasonic bath.[31] Initially, solution of ferric chloride (0.008 M) and ferrous chloride (0.016 M) from Sigma-Aldrich was mixed. To this, sodium hydroxide solution (0.5 M, 10 mL) was added in droplets at a temperature of 50°C, forming a black suspension. This suspension was sonicated for 60 minutes, then subjected to centrifugation at 15,000 rpm for 20 minutes and washed three times with deionized water. The pH of the Fe_3O_4 suspension was adjusted to 2 using a 5 M hydrochloric acid (HCl) solution, followed by another 60 minutes of sonication. The resultant Fe_3O_4 nanoparticles were stored at 4°C. The particle size and size distribution were determined by dynamic light scattering (DLS) with Zetasizer Nano ZS system (Malvern Instruments Ltd, UK). Their structural properties were characterized using a JEOL 1200 EX transmission electron microscope (TEM).[32]

Fabrication of Fe/DOX@SL Microrobots

The Fe/DOX@SL microrobots were produced using a dip-coating process.[20] Initially, 50 mg of Spora Lygodii from Kangmei Pharmaceutical Co., Ltd. was co-incubated with DOX. This mixture was then introduced to a range of Fe_3O_4 nanoparticle solutions (concentrations from 0% to 1.50%, pH=2) and agitated gently for 24 hours. The suspension was centrifuged, and the Fe/DOX@SL microrobots were collected after being washed three times with deionized water. They were then resuspended in deionized water and stored at 4°C.

Characterization of Fe/DOX@SL Microrobots

The characterization of the Fe/DOX@SL microrobots, including their TEM and energy-dispersive X-ray (EDX) imaging, was performed using the Thermo APREO S instrument (Thermo Fisher Scientific, Waltham, MA, USA). Dialysis method was used to study the release property of DOX from Fe/DOX@SL Microrobots.[33] The dialysate (release medium) was composed of PBS solutions (0.01 M, pH6.0) containing 0.5% Tween 80. An aliquot of 1 mL of Fe/DOX@SL Microrobots in different triggered conditions was added into a dialysis tubing (Snakeskin, Pierce, USA) with a cut-off molecular weight of 50kDa. At predetermined time points, 1 mL release medium was withdrawn, diluted with methanol for HPLC analysis and 1.0 mL blank release medium was immediately added into the chamber after sample collecting. The release experiment was performed in triplicate.

Cytotoxicity assay for microrobots. First, the 96-well plate was seeded with T24 tumor cells at a density of around 3000 cells each well. To determine the cytotoxicity of different groups, the cells were incubated with different concentrations. The cell viability was measured by CCK8 assay (GLPBIO) was applied for the cell viability study and the results were shown in form of average cell viability [(ODtreat-ODblank)/(ODcontrol- ODblank) × 100%] of triplicate wells.

Propulsion Investigation of Magnetic-Powered Fe/DOX@SL Microrobots

The Fe/DOX@SL microrobots were driven and guided using a custom-built magnetic field control platform comprising control and power units. The control unit, operated by LabVIEW software (version 18.0, National Instruments), generated digital signals that were converted to analog signals by a digital chip. These signals were amplified by a power amplifier (TDA8954, NXP Semiconductors) and transmitted to five electromagnetic coils (two pairs on the X and Y axes and one on the Z axis) positioned beneath an optical microscope to create an RMF.

The propulsion of the Fe/DOX@SL microrobots was examined in PBS at different magnetic frequencies and field strengths. Motion was recorded using an optical microscope equipped with a CCD camera (MS23-2, Guangzhou Mshot Photoelectric Technology) and analyzed with NIS-Elements AR 5.2 software. Further tests were conducted in biological fluids such as urine, plasma, and gastric fluid.

Animal Experiments

The animal studies were performed using 18–20 gram body weight female BALB/c nude mice, obtained from GemPharmatech Co., Ltd. All procedures were performed in accordance with the guidelines established by the Institutional Animal Care and Use Committee (IACUC) of Shenzhen Luohu Hospital Group.

In vivo Antitumor Study of Fe/DOX@SL Microrobots

An orthotopic bladder tumor model was established in mice followed by our previous published method.[2] Mice with developed T24 bladder tumors were randomly allocated into five groups, with 5 per group. These groups were treated intravesically with PBS (negative control), free Doxorubicin (DOX), free Spora Lygodii (SL), Fe/DOX@SL microrobots, and Fe/DOX@SL microrobots under RMF control (Fe/DOX@SL + RMF). DOX dosage was set at 2 mg/kg for each group. These treatments lasted for 1 hour and were administered every two days, three times in total (on days 0, 2, and 4). The treatment spanned a total of 15 days (ending on day 14).

Tumor growth was monitored through bioluminescence imaging using an LagoX system (Spectral Instruments). The mice's body weight was monitored at consistent intervals, and bioluminescence intensity and area were measured.

Following treatment, the mice were euthanized, and their bladders were removed for histological examination using hematoxylin and eosin (H&E) staining.

Statistical Analysis

A minimum of five samples was used for statistical analyses. Data are presented as mean ± standard deviation (SD). Comparisons between two groups were performed using Student's *t*-test. For comparisons involving three or more groups, one-way analysis of variance (ANOVA) with Turkey's posthoc analysis was used. All statistical evaluations were conducted using GraphPad Prism 8 software. Statistical significant differences were indicated by $^{**}p < 0.01$.

Results

Fabrication and Characterization of Fe/DOX@SL Microrobots

The preparation method of our microrobots, as illustrated in Figure 2A, builds on our previous research and involves a series of well-defined steps.[2,20] Initially, the process commences with the synthesis of Fe_3O_4 NPs. This is achieved through a chemical reaction involving ferrous chloride, ferric chloride, and sodium hydroxide. The prepared Fe_3O_4 NPs measure approximately 100 nm in size (Figure S1A) with slightly positive charge (Figure S1B). TEM images reveal their spherical morphology (Figure 2B). Prior to the preparation of microrobots, we assessed the stability of Fe_3O_4 NPs. As shown in Figure S2, the particle size of Fe_3O_4 NPs remained unchanged for more than 4 days in DMEM medium containing 10% FBS. Following this, SL undergoes two separate incubation phases: first with DOX, a chemotherapy drug, and then with the synthesized Fe_3O_4 NPs. This sequential incubation leads to the creation of the Fe/DOX@SL microrobots.

In advancing the development of Fe/DOX@SL microrobots, we focused on optimizing their preparation process. This involved experimenting with varying concentrations of Fe_3O_4 NPs during the incubation of SL. Figure 2C presents the TEM images of Fe/DOX@SL microrobots at different Fe_3O_4 NPs concentrations, including 0% (Figure 2C i), 0.25% (Figure 2C ii), 0.50% (Figure 2C iii), 0.75% (Figure 2C iv), 1.00% (Figure 2C v), 1.25% (Figure 2C vi), and 1.50% (Figure 2C vii). Our findings indicated that as the concentration of Fe_3O_4 NPs increased, there was a corresponding increase in both the coverage percentage and depth of Fe_3O_4 NPs on the SL surface. Remarkably, at a concentration of 1.00% Fe_3O_4 NPs, we observed a complete and even coverage of these NPs on the SL surface. Therefore, we determined that 1.00% is the optimal concentration for this process.

Further analysis is presented in Figure 2D. Here, the TEM image (Figure 2D i) and the EDX mappings (Figure 2D ii–iv) of the Fe/DOX@SL microrobots are showcased. The TEM image confirms a full and even coverage of the Fe_3O_4 NPs on the SL, while the EDX mappings reveal a uniform distribution of iron (Fe) elements on the SL surface. This consistent distribution is crucial for the microrobots' functionality and confirms the effectiveness of our technique in achieving a uniform coating of Fe_3O_4 NPs on the microrobots' surface, a vital step in their fabrication process. This fabrication process is pivotal in achieving the desired characteristics and efficacy of the microrobots for their intended biomedical applications.

Motion Performance of Magnetic-Propelled Fe/DOX@SL Microrobots

The manipulation and precise steering of Fe/DOX@SL microrobots were accomplished by a specially designed rotating magnetic field system. This system, as we previously reported[2,34,35] incorporates 5 electromagnetic coils arranged across X, Y and Z axes. The Fe_3O_4 NPs coating on the microrobots enables them to perform a rolling motion on surfaces when controlled by RMF.

Our investigation delved into the interaction between the propulsion behavior of Fe/DOX@SL microrobots and the frequency or intensity of the applied magnetic field. Figure 3A (Video S1) illustrates that at a constant RMF frequency of 10 hz, the microrobots' movement speed increased proportionally with the RMF intensity, reaching a maximum speed of approximately 45.9 μm/s at an intensity of 18 mT. Figure 3B presents the trajectories of these movements across various intensities, with their starting points aligned for clear comparison. We also investigated the effect of varying RMF frequencies on the microrobots' speed while maintaining a constant magnetic intensity of 18 mT (Figure 3C, Video S2). Here, the propulsion speed initially increased with frequency, then decreased, peaking at a "step-out" frequency of 9 hz.

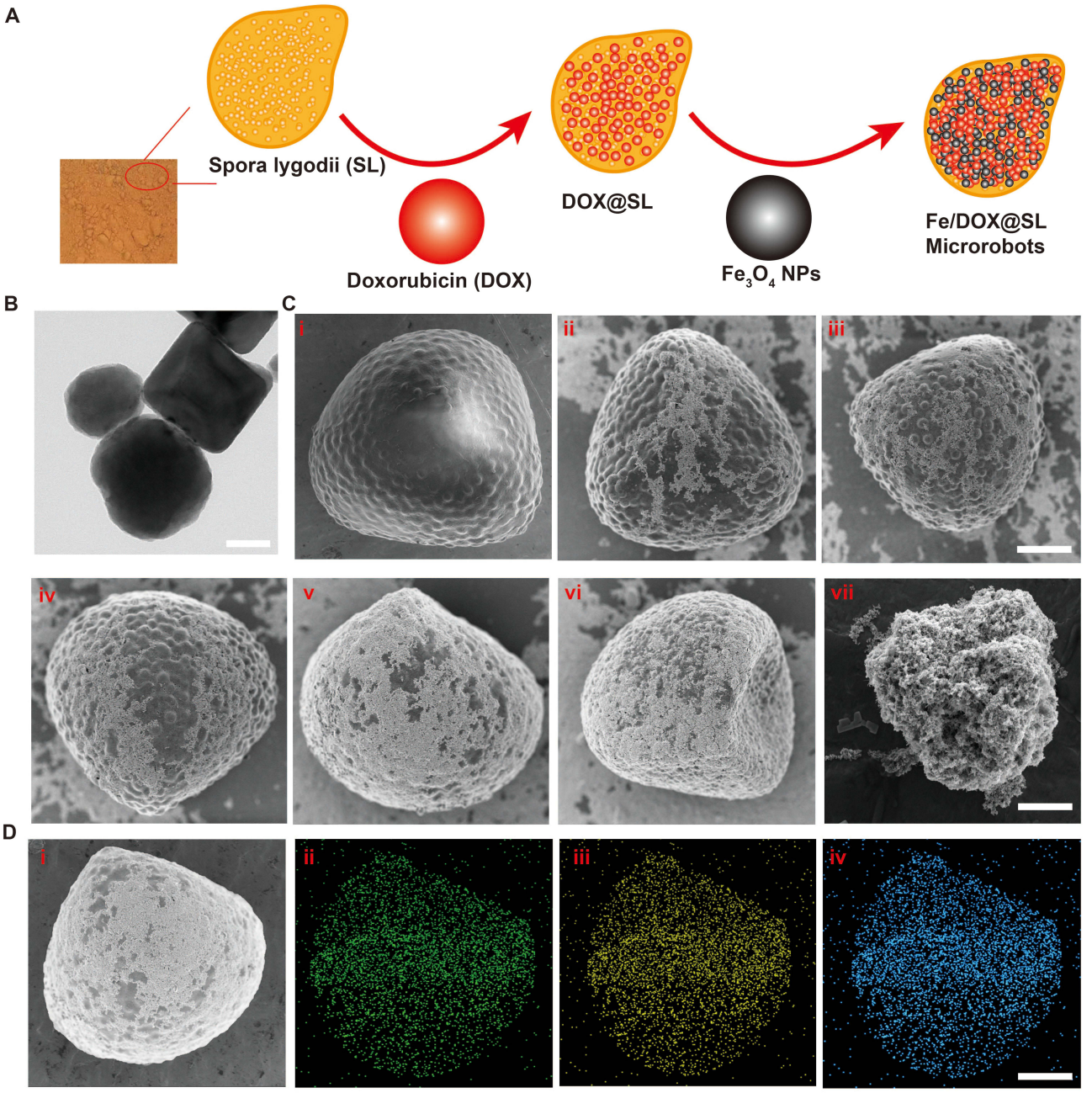

Figure 2 Preparation and characterization of Fe/DOX@SL microrobots. (**A**) Schematic illustration of the preparation process of Fe/DOX@SL microrobots. (**B**) Transmission electron microscopy (TEM) image of the Fe_3O_4 NPs. Scale Bar: 50 nm. (**C**) Scanning electron microscopy (SEM) images of the spora lygodii incubated with different concentration of Fe_3O_4 NPs, images i to vii indicated with 0%, 0.25%, 0.50%, 0.75%, 1.00%, 1.25%, and 1.50% Fe_3O_4 NPs. Scale bar: 10 μm. (**D**) SEM (i) and energy dispersive X-ray (EDX) (ii–iv, ii, C, iii, O, iv, Fe) images of the Fe/DOX@SL microrobots. Scale bar: 10 μm.

The trajectories corresponding to these varying frequencies are illustrated in Figure 3D. The propulsion performance of the microrobots was also tested in different fluids to simulate different biologically applied fields, as shown in Figure 3E (Video S3). The microrobots exhibited effective controlled actuation in diverse media including DI water, PBS, gastric fluid, simulated urine, and plasma. This demonstrates the robustness of the Fe_3O_4 NPs encapsulation on SL and the microrobots' adaptability to different environments. The corresponding movement trajectories are presented in Figure 3F. Moreover, the closed-loop control of our magnetic actuation system enables precise navigation of the Fe/DOX@SL microrobots along predefined paths. As illustrated in Figure 3G (Video S4), the microrobots followed a square-like trajectory, controlled by changing the orientation of the applied RMF. Overall, these results indicate that the Fe/

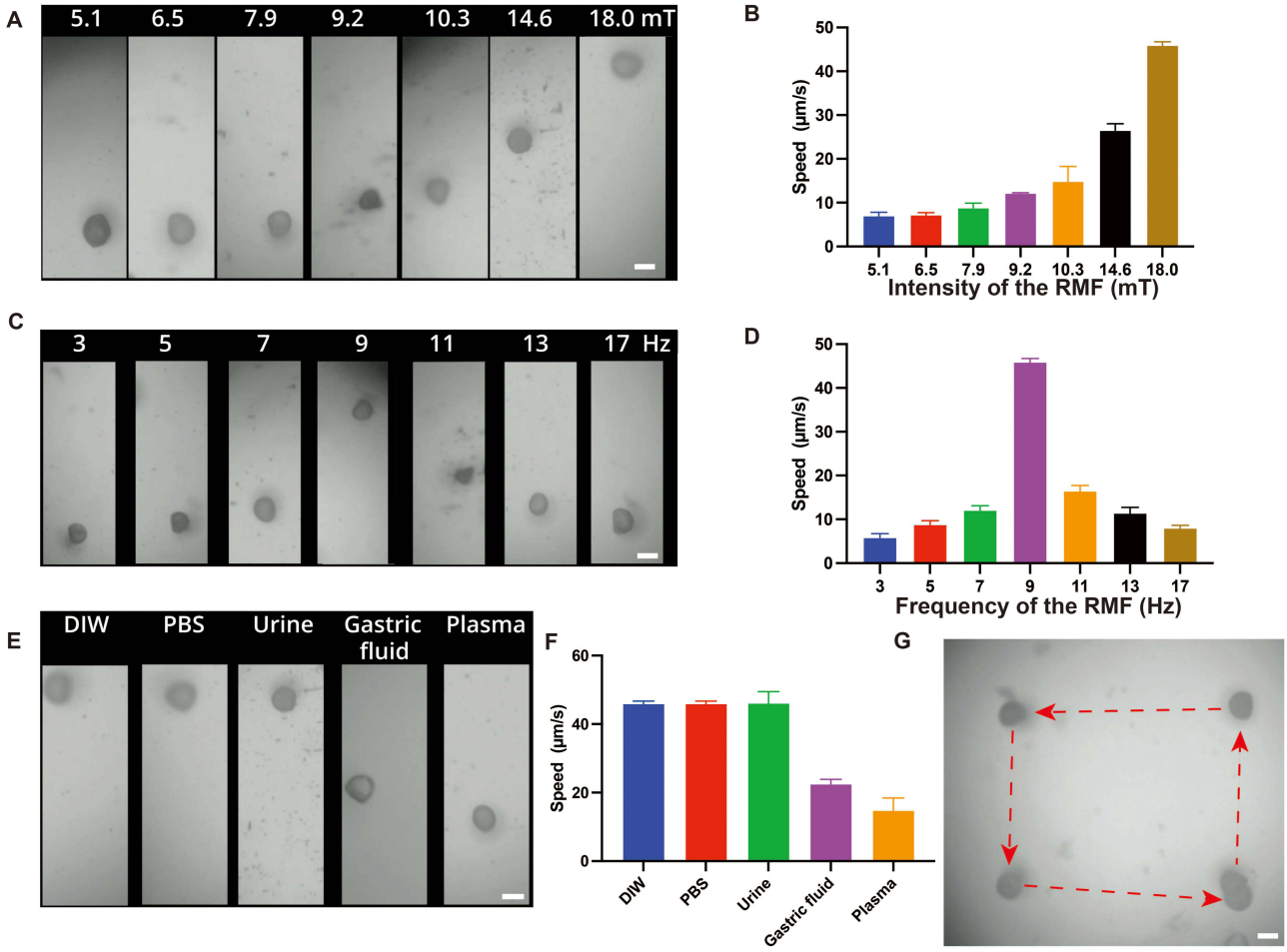

Figure 3 Locomotion performance of magnetic-propelled Fe/DOX@SL microrobots. Movement speed (**A**) and corresponding time-lapse visuals displaying paths over 3 seconds (**B**) of microrobots subjected to rotating magnetic field (RMF) at varying field strengths, with a constant frequency of 10 hz. Scale bar: 10 μm (n = 5; mean ± SD). Movement speed (**C**) and time-lapse visuals with paths over 3 seconds (**D**) of microrobots under different RMF frequencies, while keeping the field strength steady at 18 mT. Scale bar: 10 μm (n = 5; mean ± SD). Movement speed (**E**) and time-lapse visuals showing paths over 3 seconds (**F**) of microrobots in various environments, under RMF conditions of 18 mT and 9 hz. Scale bar: 10 μm (n = 5; mean ± SD). (**G**) Movement paths of magnetically driven microrobots following a predefined square-like route (18 mT, 9 hz). Scale bar: 10 μm.

DOX@SL microrobots are capable of efficient and controllable movement in various biological media under RMF control, showcasing their potential for diverse biomedical applications.

Treatment Efficacy of Fe/DOX@SL Microrobots Against Bladder Cancer

Having established the controlled motion of Fe/DOX@SL microrobots under our customized RMF, we next investigated the microrobots' in vivo therapeutic effectiveness against bladder cancer. Before evaluating the in vivo antitumor effects, we conducted in vitro assessments of the microrobots' cytotoxicity and biocompatibility. The drug release profile revealed that approximately 50% of the loaded DOX was released within the first 6 hours, reaching nearly 90% after 24 hours (Figure S3). This sustained release pattern is expected to significantly reduce the systemic side effects of DOX while maintaining a prolonged therapeutic effect. Cell viability assays showed that Fe/DOX@SL microrobots exhibited lower cytotoxicity compared to free DOX (Figure S4), which aligns with the controlled and gradual release of the drug. Additionally, the Fe/DOX@SL microrobots demonstrated excellent biocompatibility, as indicated by their minimal hemolytic activity (<0.1%), in stark contrast to the 100% hemolysis observed with distilled water (Figure S5). These results highlight the safety and potential of Fe/DOX@SL microrobots as a biocompatible and effective platform for targeted cancer therapy.

Balb/c nude mice with orthotopic bladder cancer were first build by surgically implanting T24 cells with luciferase reporter onto the bladder wall. After a week of recovery, the mice with established T24 bladder cancer were randomly allocated into five groups with five mice each group), and treated with various agents: PBS (as a negative control), free Doxorubicin (DOX), free Spora Lygodii, Fe/DOX@SL microrobots, and Fe/DOX@SL microrobots under RMF control (Fe/DOX@SL + RMF) at an intensity of 18.0 mT and frequency of 9 hz (Figure 4A). These treatments were administered intravesically for one hour, repeated on days 1 and 3. Tumor progression was monitored through the bioluminescence emitted by the luciferase. As shown in Figure 4B, by day 13, the group treated with free SL showed tumor growth similar to the PBS control group. However, a decrease in tumor growth was noted in the group treated with free DOX. This therapeutic effect was further enhanced with the intravesical injection of Fe/DOX@SL microrobots. The most substantial decrease in tumor growth was witnessed in mice treated with Fe/DOX@SL microrobots under RMF control (Fe/DOX@SL+ RMF). The bioluminescence intensity in this group was significantly lower than in the free DOX and Fe/DOX@SL groups, suggesting enhanced anti-cancer efficacy due to prolonged retention of the microrobots in the bladder. This group also exhibited the smallest bioluminescence area at the treatment's conclusion, indicative of the most effective tumor suppression. Representative bioluminescence images in Figure 4C clearly show the lowest intensity and smallest tumor area in the Fe/DOX@SL + RMF group on day 13. Post-treatment analysis of the mice bladders through hematoxylin and eosin (H&E) staining (Figure 4D) further confirmed the significant reduction of the bladder tumors in the Fe/DOX@SL + RMF group compared to the other treatments. Overall, these findings underscore the superior anti-tumor efficacy of Fe/DOX@SL microrobots when guided by magnetic manipulation. This approach not only enhances

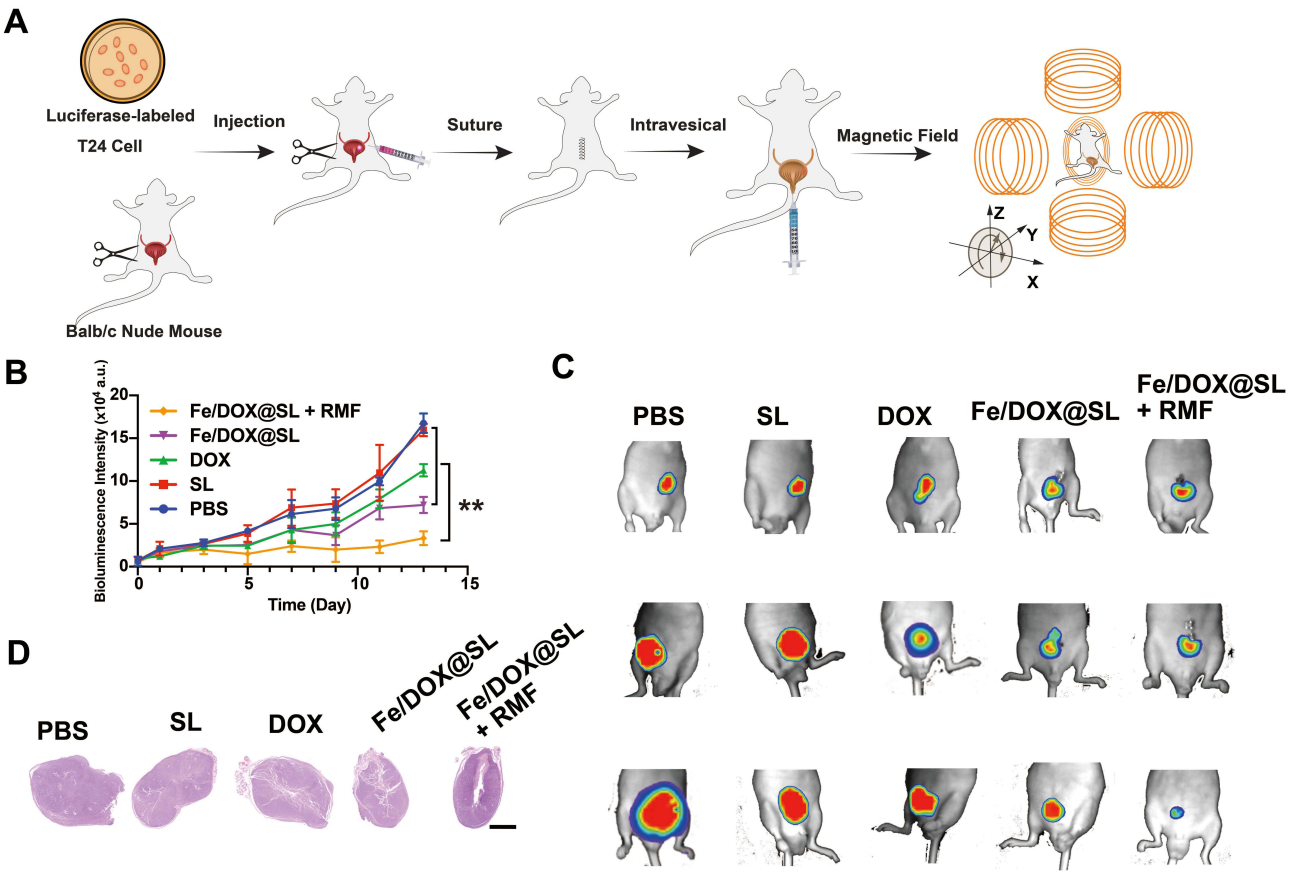

Figure 4 In vivo therapeutic effectiveness of Fe/DOX@SL microrobots against bladder cancer. (**A**) Diagram of the experimental protocol for establishing orthotopic T24 bladder tumors in Balb/c nude mice, followed by different intravesical treatments. Bioluminescence intensity (**B**) and representative in vivo bioluminescence images (**C**) of T24 tumor-bearing mice under various intravesical treatments, including PBS (negative control), free SL, free DOX, Fe/DOX@SL microrobots, and Fe/DOX@SL microrobots under RMF guidance (Fe/DOX@SL microrobots + RMF) (18 mT, 9 hz), throughout the treatment course. (n = 5; mean ± SD). **P < 0.01; ANOVA. (**D**) Hematoxylin and eosin (H&E) staining of bladder tumor sections from T24 tumor-bearing mice at the end of the treatment period (Day 13) following different intravesical treatments. Scale bar: 3 mm.

the therapeutic impact but also demonstrates promising biosafety profiles, paving the way for advanced treatments for orthotopic bladder tumors.

Discussion and Conclusion

This study successfully demonstrated the innovative fusion of Traditional Chinese Medicine and advanced microrobotics, culminating in the development of a novel therapeutic platform for bladder cancer therapy. The key component of this platform is Spora Lygodii, a TCM element known for its therapeutic properties, combined with the modern technology of microrobotics. The encapsulation of DOX and Fe_3O_4 nanoparticles within SL's porous structure led to the creation of Fe/DOX@SL microrobots, able to achieve accurate, stable, and directed movement in diverse biological settings when guided by an external RMF. The significant advancement lies in the ability of these microrobots to navigate and remain within the bladder, providing targeted therapy through enhanced adherence to the bladder mucosa and increased retention time. This targeted approach has shown a significantly improved anti-tumor effect in mouse models with T24 bladder tumors, outperforming other passive treatment methods. By harnessing the intrinsic healing properties of SL spores and integrating them with a fuel-free, controllable propulsion mechanism, this research has opened new avenues for the effective treatment of bladder tumor.

This study builds upon and surpasses previous advancements in microrobots for targeted drug delivery by addressing critical limitations. Earlier efforts, such as urease-powered micromotors for bladder cancer spheroid targeting,[25] demonstrated propulsion capabilities but relied on chemical fuels like urea. These enzymatic micromotors faced significant challenges, including limited in vivo applicability due to their dependency on chemical fuels and lack of precise propulsion control. In contrast, our Fe/DOX@SL microrobots utilize fuel-free magnetic propulsion, offering a safer and more controllable alternative for targeted drug delivery.

Moreover, studies employing diatom-based microrobots targeting,[36] have showcased the potential of porous natural structures for drug delivery but were constrained by the absence of biocompatible and efficient propulsion systems. The Fe/DOX@SL microrobots overcome these limitations by leveraging the natural porosity of Spora Lygodii (SL) spores for efficient drug loading and integrating a magnetic coating for precise navigation. This unique combination allows for enhanced adherence to the bladder mucosa and prolonged retention, effectively addressing the challenges faced by earlier designs.

A significant advancement of this work is the ability of Fe/DOX@SL microrobots to navigate and remain within the bladder under magnetic guidance, providing targeted therapy through improved mucosal adherence and retention. These innovations result in markedly enhanced anti-tumor effects in mouse models with T24 bladder tumors, demonstrating the platform's ability to outperform traditional passive treatments.

By harnessing the intrinsic therapeutic properties of SL spores and combining them with a fuel-free, controllable propulsion mechanism, this study opens new avenues for the effective treatment of bladder tumors. The biocompatibility and biodegradability of the microrobots further enhance their potential for clinical applications, making them a promising candidate for translational research.

Future work will focus on optimizing the Fe/DOX@SL microrobots for clinical translation. Key priorities include refining the fabrication process for scalability, enhancing microrobot stability and biodegradability in human biological environments, and conducting preclinical studies to evaluate long-term biosafety and therapeutic efficacy. Additionally, the integration of real-time imaging techniques for in vivo monitoring and the adaptation of this platform for treating other localized cancers will be explored. These efforts aim to bridge the gap between experimental research and clinical applications, paving the way for more effective and targeted therapeutic strategies in the future.

Ethics Approval

All procedures were performed in accordance with the guidelines established by the Institutional Animal Care and Use Committee (IACUC) of Shenzhen Luohu Hospital Group. All experimental protocols were reviewed and approved by the IACUC of Shenzhen Luohu Hospital Group (No: 2022-SZZQ-09-012).

Funding

This research was funded by the National Natural Science Foundation Fund of China, grant number 32101133; Shenzhen Science and Technology Program, grant numbers JCYJ20210324125006019, and RCBS20221008093125067.

Disclosure

The author(s) report no conflicts of interest in this work.

References

1. Wang X, Chen XZ, Alcântara CC, et al. MOFBOTS: metal–organic-framework-based biomedical microrobots. *Adv Mater*. 2019;31(27):1901592. doi:10.1002/adma.201901592
2. Cong Z, Tang S, Xie L, et al. Magnetic-powered janus cell robots loaded with oncolytic adenovirus for active and targeted virotherapy of bladder cancer. *Adv Mater*. 2022;34(26):2201042. doi:10.1002/adma.202201042
3. Peng X, Urso M, Ussia M, Pumera M. Shape-controlled self-assembly of light-powered microrobots into ordered microchains for cells transport and water remediation. *ACS Nano*. 2022;16(5):7615–7625. doi:10.1021/acsnano.1c11136
4. Li J, Yu J. Biodegradable microrobots and their biomedical applications: a review. *Nanomaterials*. 2023;13(10):1590. doi:10.3390/nano13101590
5. Wang S, Xu J, Zhou Q, et al. Biodegradability of micro/nanomotors: challenges and opportunities. *Adv Healthc Mater*. 2021;10(13):2100335. doi:10.1002/adhm.202100335
6. Wang Y, Shen J, Handschuh-Wang S, Qiu M, Du S, Wang B. Microrobots for targeted delivery and therapy in digestive system. *ACS Nano*. 2022;17(1):27–50. doi:10.1021/acsnano.2c04716
7. Soto F, Karshalev E, Zhang F, Esteban Fernandez de Avila B, Nourhani A, Wang J. Smart materials for microrobots. *Chem Rev*. 2021;122(5):5365–5403. doi:10.1021/acs.chemrev.0c00999
8. Terzopoulou A, Wang X, Chen XZ, et al. Biodegradable metal–organic framework-based microrobots (MOFBOTs). *Adv Healthc Mater*. 2020;9(20):2001031. doi:10.1002/adhm.202001031
9. Park J, Jin C, Lee S, Kim JY, Choi H. Magnetically actuated degradable microrobots for actively controlled drug release and hyperthermia therapy. *Adv Healthc Mater*. 2019;8(16):1900213. doi:10.1002/adhm.201900213
10. Pena-Francesch A, Giltinan J, Sitti M. Multifunctional and biodegradable self-propelled protein motors. *Nat Commun*. 2019;10(1):3188. doi:10.1038/s41467-019-11141-9
11. Maria-Hormigos R, Mayorga-Martinez CC, Pumera M. Soft magnetic microrobots for photoactive pollutant removal. *Small Methods*. 2023;7(1):2201014. doi:10.1002/smtd.202201014
12. Sinha A, Simnani FZ, Singh D, et al. The translational paradigm of nanobiomaterials: biological chemistry to modern applications. *Mater Today Bio*. 2022;17:100463. doi:10.1016/j.mtbio.2022.100463
13. Fu L, Wang Y, Zhao Y, Huang L. The concept of traditional Chinese medicine: history, theory and empirical research. *Zhonghua yi shi za zhi*. 2022;52(4):195–205. doi:10.3760/cma.j.cn112155-20220516-00062
14. Zhang SQ, Li JC. An introduction to traditional Chinese medicine, including acupuncture. *Anat Rec*. 2021;304(11):2359–2364. doi:10.1002/ar.24782
15. Jiang C-H, Sun T-L, Xiang D-X, Wei -S-S, Li W-Q. Anticancer activity and mechanism of xanthohumol: a prenylated flavonoid from hops (Humulus lupulus L.). *Front Pharmacol*. 2018;9:530. doi:10.3389/fphar.2018.00530
16. Sun D, Li X, Nie S, Liu J, Wang S. Disorders of cancer metabolism: the therapeutic potential of cannabinoids. *Biomed Pharmacother*. 2023;157:113993.
17. Xiong X, Yang X, Liu Y, Zhang Y, Wang P, Wang J. Chinese herbal formulas for treating hypertension in traditional Chinese medicine: perspective of modern science. *Hypertens Res*. 2013;36(7):570–579. doi:10.1038/hr.2013.18
18. Mundargi RC, Potroz MG, Park S, et al. Lycopodium spores: a naturally manufactured, superrobust biomaterial for drug delivery. *Adv Funct Mater*. 2016;26(4):487–497. doi:10.1002/adfm.201502322
19. Diego-Taboada A, Maillet L, Banoub JH, et al. Protein free microcapsules obtained from plant spores as a model for drug delivery: ibuprofen encapsulation, release and taste masking. *J Mat Chem B*. 2013;1(5):707–713. doi:10.1039/c2tb00228k
20. Yang Q, Tang S, Lu D, et al. Pollen typhae-based magnetic-powered microrobots toward acute gastric bleeding treatment. *ACS Appl Bio Mater*. 2022;5(9):4425–4434. doi:10.1021/acsabm.2c00565
21. Siegel RL, Miller KD, Wagle NS, Jemal A. Cancer statistics, 2023. *Ca Cancer J Clin*. 2023;73(1):17–48. doi:10.3322/caac.21763
22. Compérat E, Amin MB, Cathomas R, et al. Current best practice for bladder cancer: a narrative review of diagnostics and treatments. *Lancet*. 2022;400(10364):1712–1721. doi:10.1016/S0140-6736(22)01188-6
23. Liu S, Chen X, Lin T. Emerging strategies for the improvement of chemotherapy in bladder cancer: current knowledge and future perspectives. *J Adv Res*. 2022;39:187–202. doi:10.1016/j.jare.2021.11.010
24. Burdett S, Fisher DJ, Vale CL, et al. Adjuvant chemotherapy for muscle-invasive bladder cancer: a systematic review and meta-analysis of individual participant data from randomised controlled trials. *Europ urol*. 2022;81(1):50–61. doi:10.1016/j.eururo.2021.09.028
25. Hortelao AC, Carrascosa R, Murillo-Cremaes N, Patino T, Sanchez S. Targeting 3D bladder cancer spheroids with urease-powered nanomotors. *Acs Nano*. 2018;13(1):429–439. doi:10.1021/acsnano.8b06610
26. Nie Y, Li D, Peng Y, et al. Metal organic framework coated MnO2 nanosheets delivering doxorubicin and self-activated DNAzyme for chemo-gene combinatorial treatment of cancer. *Int J Pharm*. 2020;585:119513. doi:10.1016/j.ijpharm.2020.119513
27. Zhang W, Zheng X, Shen S, Wang X. Doxorubicin-loaded magnetic nanoparticle clusters for chemo-photothermal treatment of the prostate cancer cell line PC3. *Biochem Biophys Res Commun*. 2015;466(2):278–282. doi:10.1016/j.bbrc.2015.09.036
28. Sheel R, Kumari P, Panda PK, et al. Molecular intrinsic proximal interaction infer oxidative stress and apoptosis modulated in vivo biocompatibility of P. niruri contrived antibacterial iron oxide nanoparticles with zebrafish. *Environ Pollut*. 2020;267:115482. doi:10.1016/j.envpol.2020.115482

29. Xi S, Gong Y. *Essentials of Chinese Materia Medica and Medical Formulas: New Century Traditional Chinese Medicine*. Academic Press; 2017.
30. Kim Y-S, Song J-H, Choi G, Lee G, Ju Y-S. Comparative study on the external micro-morphology of 3 kinds of minute pollen and spore Herbs (Pini Pollen, Typhae Pollen, Lygodii Spora) utilizing scanning electron microscope. *Korea J Herbol*. 2020;35(1):9–18.
31. Ayed SB, Sbihi H, Azam M, Al-Resayes S, Ayadi M, Ayari F. Local iron ore identification: comparison to synthesized Fe3O4 nanoparticles obtained by ultrasonic assisted reverse co-precipitation method for Auramine O dye adsorption. *Desalin Water Treat*. 2021;220:446–458. doi:10.5004/dwt.2021.27080
32. Cong Z, Zhang L, Ma S-Q, Lam KS, Yang -F-F, Liao Y-H. Size-transformable hyaluronan stacked self-assembling peptide nanoparticles for improved transcellular tumor penetration and photo–chemo combination therapy. *ACS Nano*. 2020;14(2):1958–1970. doi:10.1021/acsnano.9b08434
33. Cong Z, Yang F, Cao L, et al. Multispectral optoacoustic tomography (MSOT) for imaging the particle size-dependent intratumoral distribution of polymeric micelles. *Int J Nanomed*. 2018;Volume 13:8549–8560. doi:10.2147/IJN.S185726
34. Li Y, Cong Z, Xie L, et al. Magnetically powered immunogenic macrophage microrobots for targeted multimodal cancer therapy. *Small*. 2023;19 (42):2301489. doi:10.1002/smll.202301489
35. Xie L, Cong Z, Tang S, et al. Oncolytic adenovirus-loaded magnetic-driven Janus tumor cell robots for active and targeted virotherapy of homologous carcinoma. *Mater Today Chem*. 2023;30:101560. doi:10.1016/j.mtchem.2023.101560
36. Li M, Wu J, Lin D, et al. A diatom-based biohybrid microrobot with a high drug-loading capacity and pH-sensitive drug release for target therapy. *Acta Biomater*. 2022;154:443–453. doi:10.1016/j.actbio.2022.10.019